Thermal evolution of crystal shapes: The fcc crystal

C. Jayaprakash and W. F. Saam
Department of Physics, The Ohio State University, Columbus, Ohio 43210
(Received 29 May 1984)

The thermal evolution of the equilibrium shape of an fcc crystal with both first- and second-nearest-neighbor interatomic interactions is studied. Exact zero-temperature calculations are extended to nonzero temperatures by use of solid-on-solid models appropriate to ⟨001⟩ and ⟨110⟩ directions in the crystal, yielding a reasonably complete global description of the thermal evolution. Universal features of the shape associated with second-order phase transitions are described, as are first-order phase transitions which appear as sharp edges between facets. Some new results for the six-vertex model appear as by-products. Contact is made with experiment, including a discussion of practical limitations on measurements of universal features of crystal shapes.

I. INTRODUCTION

At a first-order transition between a solid and a fluid, a macroscopic crystal can coexist in stable equilibrium with its fluid. The equilibrium shape of the crystal is determined by minimizing the interfacial free energy (free-energy cost of creating the boundaries) for a fixed volume of the crystal. The dependence of the interfacial free energy (or surface tension) on the orientation of the particular plane due to crystalline anisotropy gives rise to complex shapes. The crystal may be a polyhedron, i.e., made up of planar surfaces (facets), or may be rounded, i.e., made up entirely of curved surfaces, or be a combination of facets and smoothly curved faces. Normally, at $T=0$ the crystal is completely faceted and becomes rounded at sufficiently high temperature (but still below the melting temperature). In this paper we trace this evolution for an fcc lattice with near-neighbor $(-J_1)$ and next-near-neighbor $(-J_2 \equiv -RJ_1)$ interactions via mappings onto the two-dimensional six-vertex model and exploiting the known exact solution. Specifically, the interfacial free energy is obtained by making the correspondence and then used in the determination of the crystal shape. These mappings focus on specific symmetry planes and can only describe small tilt angles with respect to them. Taken together with the exact zero-temperature shape for the whole crystal, they provide a semiquantitaive global description of the crystal shape for nonzero temperatures as a function of R.

In recent important work, Rottman and Wortis[1,2] (RW) have studied this problem directly in three dimensions for a simple-cubic-lattice model within the mean-field approximation (MFA). However, the phenomenon of roughening[3] is absent within the MFA, and they obtain detailed descriptions of the crystal shape by supplementing the MFA results with features which depend critically on fluctuations in a very plausible way. In contrast, our results are based on the exact solution of a model that includes roughening. However, our model has the so-called solid-on-solid constraint[4] which excludes bulk excitations and overhangs. Thus the model is applicable only for small tilt angles (see Secs. IV and V) while RW can directly treat the entire crystal. We provide a detailed comparison of our results with those of RW and comment on the differences.

In addition to the global picture, our results include all the universal features pertaining to specific local properties reported earlier.[5,6] We briefly summarize our results: When two faces of an equilibrium crystal meet the slopes can change either continuously (second-order phase transition) or discontinuously (first-order phase transition). Within our model, the transitions from curved to flat faces are always continuous (in contrast to RW)[1,2] and are in the universality class of the Pokrovsky-Talapov[7] (PT) type, leading to an exponent $\frac{3}{2}$ (Ref. 8) describing the way in which the curved part meets the facet (see Sec. V). This prediction, made independently by Rottman and Wortis,[1,2] has in fact been verified in lead crystals.[9]

When the next-nearest-neighbor interactions are attractive, we find that a sharp edge between facets can persist at finite temperatures, corresponding to a first-order phase transition. When this edge is approached from neighboring curved (rough) regions, there is also a first-order phase transition, signaled in the crystal shape by a slope discontinuity. The ends of the edge trace, as a function of temperature, a first-order phase boundary that has apparently previously gone unnoticed in the six-vertex model.

In addition, the thermal evolution of facets is traced, and at the roughening temperature the facets disappear with an associated universal jump in the curvature of $2/\pi$ in appropriate units (see Sec. V). This jump has recently been seen by Gallet, Wolf, and Balibar[10] in elegant experiments on hcp ^{4}He crystals. Thus a rather complete picture of the crystal shape emerges from these model calculations.

The paper is organized as follows: Section II gives a brief review of crystal-shape theory including the Wulff construction. In Sec. III the $T=0$ crystal shape is discussed. A summary of the relevant details of the six-vertex model can be found in Sec. IV. Section V gives a detailed account of our results for different signs of the next-nearest-neighbor interactions, along with appropriate comparisons with RW. Remarks regarding the experi-

mental aspects of observing our predictions are provided in Sec. VI. Some technical details of the derivation of six-vertex model results not found in the literature are outlined in the Appendix.

II. REVIEW OF CRYSTAL-SHAPE THEORY

When a macroscopic amount of a solid coexists in equilibrium with a fluid which surrounds it, the shape of the interior region is obtained by minimizing the surface integral of the interfacial free-energy density $\sigma(\hat{n},T)$ subject to the constraint of fixed volume. In general $\sigma(\hat{n},T)$ depends on the orientation $\hat{n}$ of the surface with respect to some natural axes fixed in the crystal. Mathematically stated, one minimizes[11]

$$\int \sigma(\hat{n},T)dS - 2\lambda \int dV ,$$

where 2λ is the Lagrange multiplier; if P_s and P_f are, respectively, the pressures in the solid and fluid phases, then[12,13]

$$2\lambda = P_s - P_l > 0 . \tag{1}$$

The minimization procedure leads to the Wulff construction for $R(\hat{r})$ and the radius of the equilibrium crystal shape (ECS) in the direction $\hat{r}$; analytically stated

$$\lambda R(\hat{r}) = \min_{\hat{n}} \frac{\sigma(\hat{n})}{\hat{n}\cdot\hat{r}} . \tag{2}$$

Geometrically this is equivalent to the following elegant construction: Make a polar plot of $\sigma(\hat{n},T)$ as a function of $\hat{n}$ and draw a radius in the direction $\hat{n}$ from the origin to a point of the plot. Then construct a plane perpendicular to the given $\hat{n}$ which passes through the intersection of the radius with the plot. Do this for all directions $\hat{n}$; then the interior envelope of all such planes yields the ECS $R(\hat{r})$. Cusps in this plot naturally lead to extended planar regions (facets) of the crystal. Further, edges and corners of the ECS may be degenerate in the sense that many planes from the Wulff construction may pass through them.

For our purposes it is convenient to focus on a particular direction $\hat{n}_z$ and to define, following Landau[11] and Andreev,[14] the ECS by $z(\vec{r})$, the height of the surface with respect to the plane $\vec{r}=(x,y)$. Then we must minimize

$$\int\int dx\,dy[f(\vec{s})-2\lambda z(\vec{r})] ,$$

where $\vec{s}=\vec{\nabla}z(\vec{r})$, $f(\vec{s})=\sigma(\vec{s})[1+|\vec{s}|^2]^{1/2}$ is the interfacial free energy $\sigma(\vec{s})$, projected onto the x-y plane, and 2λ is the previous Lagrange multiplier. The solution to this variational problem is most conveniently expressed in terms of the Legendre-transformed potential

$$\tilde{f}(\vec{\eta}) = \min_{\vec{s}} [f(\vec{s}) - \vec{\eta}\cdot\vec{s}] , \tag{3}$$

where $\vec{\eta}=\partial f/\partial \vec{s}$; the ECS is then given by[14]

$$\lambda z(\vec{r}) = \tilde{f}(-\lambda\vec{r}) . \tag{4}$$

We will use Eq. (2) to analyze the $T=0$ ECS and to make some qualitative predictions for $T>0$. Equation (4) will be used in connection with a solid-on-solid (SOS) model[4] which can be mapped onto the six-vertex model[15–17] to study the thermal evolution of the ECS near certain principal facets, corners, and edges.

III. THE $T=0$ CRYSTAL SHAPE

Consider a face-centered-cubic lattice with nearest-neighbor interactions $-J_1$ and next-nearest-neighbor interactions $-J_2$. We always assume $J_1>0$ (attractive interaction). As we shall see, a study of the zero-temperature interfacial free energy $\sigma_0(\vec{k})$ of the $\vec{k}=(h,k,l)$ plane provides not only the $T=0$ crystal shape via the Wulff construction, but suggests the qualitative behavior of the shape as a function of T.

Mackenzie *et al.*[18] have provided the explicit expression

$$\sigma_0(\vec{k}) = \frac{J_1}{\Omega}\frac{\vec{k}}{|\vec{k}|}\cdot[[2,1,0]+R[1,1,1]] \tag{5}$$

for $h\geq k\geq l$, other directions following from symmetry considerations. Also, $R\equiv J_2/J_1$ and Ω, the volume per atom is $a^2/4$, a being the cubic-unit-cell lattice constant. The planes of primary interest to us here are (100), (110), and (111), and from Eq. (5),

$$\begin{aligned}
\sigma_0((1,0,0)) &= \left[\frac{a^2}{4}\right]^{-1}(2J_1+J_2) ,\\
\sigma_0((1,1,0)) &= \left[\frac{a^2}{\sqrt{2}}\right]^{-1}(6J_1+4J_2) ,\\
\sigma_0((1,1,1)) &= (\sqrt{3}a^2)^{-1}(12J_1+12J_2) .
\end{aligned} \tag{6}$$

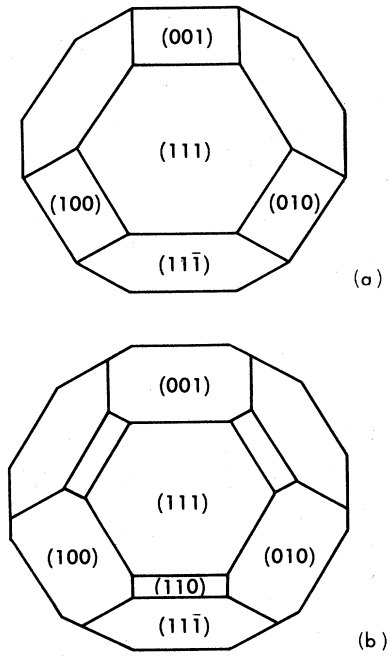

FIG. 1. $T=0$ shapes for the fcc crystal with (a) $J_2/J_1=0$ and (b) $J_2/J_1=+0.1$. The shape for $J_2/J_1=-0.1$ differs from (a) only quantitatively in that facet sizes are slightly different for the two cases.

For the case $R=0$, only the (100) and (111) planes (and their symmetry equivalents) appear, with finite size, in the equilibrium crystal shape shown in Fig. 1(a). All planes with $h \geq k \geq l$ contribute to the point of intersection of the (100), (111), and (11$\bar{1}$) planes. All planes with $h=k>0$ contribute to the edge separating the (111) and (11$\bar{1}$) planes, while all planes with $h \geq k=l \geq 0$ contribute to the edge separating the (100) and (111) planes. Thus the edges and intersection points are highly degenerate at $T=0$. In the Andreev[14] picture there are, correspondingly, many configurations (facets) with the same $f(\vec{\eta})$ if $\vec{\eta}$ is restricted to edges. If the temperature is raised slightly from $T=0$, it is plausible to expect that entropy effects will remove the degeneracy and that all facets will appear, producing rough portions on the crystal surface. This in fact happens in the model calculations presented later.

For the case $R>0$, the (110) facet appears (with aspect ratio, height/width $=R/\sqrt{2}$) in addition to the (100) and (111) facets, as seen in Fig. 1(b). All other facets contribute to the degeneracies at edges and/or corners. Once again we anticipate that raising T will remove the degeneracy, a feature observed in our exact calculation.

The case $R<0$ is quite interesting. Here the shape remains as in Fig. 1(a); only the (100) and (111) facets appear. The degeneracy along the edge between (111) and (11$\bar{1}$) is removed [only (111) and (11$\bar{1}$) have the same $\tilde{f}(\vec{\eta})$ at the edge]. The earlier degeneracy along the edge between (111) and (100) remains. The point of intersection between (100), (111), and (11$\bar{1}$) retains only the degeneracy of the (100)-(11$\bar{1}$) edge [plus that of the (100)-(111) edge]. These facts are easily confirmed if we compute, via Herring's technique,[19] the energy of an arbitrary $(h\,k\,l)$ plane, assuming it breaks up (facets) into an appropriate coexistence mixture of (100), (111), and (11$\bar{1}$) planes. This energy, $\sigma_0^f(\vec{k})$, is

$$\sigma_0^f(\vec{k})=\frac{J_1}{\Omega}\frac{\vec{k}}{|\vec{k}|}\cdot[[2,1,0]+R[1,2,0]] . \tag{7}$$

Then

$$\sigma_0(\vec{k})-\sigma_0^f(\vec{k})=\frac{J_2}{|\vec{k}|\Omega}(l-k) , \tag{8}$$

which is positive (>0) for $J_2<0$, $k \geq l$. Only for $k=l$, i.e., the (100)-(111) edge, do planes other than (100) and (111) remain degenerate and thus stable. All others are not stable. For $R<0$ then we expect the (100)-(111) edge to vanish at $T>0$ as entropy effects immediately remove the degeneracy. The (111)-(11$\bar{1}$) edge is, however, expected to remain until some finite temperature at which free-energy barriers can be overcome allowing all planes with $h=k$ to appear. This scenario is followed in our exact model calculations of Sec. V.

To briefly summarize our qualitative picture derived from $T=0$ results, degenerate edges will vanish for any $T>0$, nondegenerate ones at some finite $T>0$. Further, facets appearing with finite area at $T=0$ are expected to disappear (roughen) at characteristic nonzero temperatures; this expectation comes from our earlier results.[5,6]

IV. THE SIX-VERTEX MODEL

Here we describe the six-vertex SOS models which we shall employ to study the thermal evolution of the fcc crystal with both nearest- and next-nearest-neighbor interactions. These models are adaptations to the fcc case of the original body-centered solid-on-solid model constructed by van Beijeren,[20] and used by us earlier[5,6] to study facet formation in bcc crystals with nearest-neighbor interactions only.

A solid-on-solid model[4] can be defined for a given interface [e.g., with Miller indices (100) or (110)] as a model which excludes voids (bulk excitations) and overhangs. The free energy of the interface is computed by taking a trace only over those configurations which satisfy these SOS conditions.[21]

Consider first the (110) face. Following van Beijeren[20] the SOS model for this face can be mapped onto the six-vertex model, as illustrated in Fig. 2. The relevant bonds are $-J_2$ vertically and $-J_1$ horizontally. The closed circles indicate atoms in the top plane, while open circles indicate atoms in the next plane down. A vertex corresponds to a set of two closed and two open circles. A minus sign indicates a vacancy at the corresponding atomic site, all atoms below this site being present. Viewed from the (110) direction there are two equivalent ground states, with energies e_5 and e_6, the former state being related to the latter by removal of the top layer of atoms. The excited-state vertices, with energies e_1 through e_4, correspond to local tilts away from the [110] direction, and the slopes s_x and s_y in the x and y directions are indicated in Fig. 2. The fields $\tilde{A}\eta_x$ and $\tilde{A}\eta_y$ ($\tilde{A}=a^2/\sqrt{2}$ being the area per vertex) of the figure are related to the original horizontal and vertical electric fields $\mathscr{H}$ and $\mathscr{V}$ of the six-vertex model[15] by

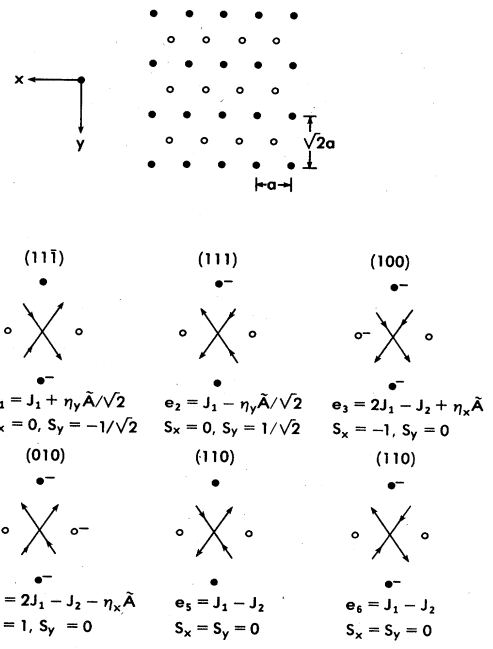

FIG. 2. Mapping of the six-vertex model onto the (110) face of an fcc crystal. See Sec. IV for notation.

$$\mathscr{H}=-\frac{\tilde{A}}{2}(\eta_x+\eta_y/\sqrt{2}) ,$$
$$\mathscr{V}=-\frac{\tilde{A}}{2}(\eta_x-\eta_y/\sqrt{2}) . \tag{9}$$

From the results of Secs. II and III it is straightforward to show that the projected interfacial energies $f(\vec{s})$ for the (110), (100), and (111) facets are, at $T=0$,

$$f_{110}\tilde{A}=3J_1+2J_2 ,$$
$$f_{100}\tilde{A}=4J_1+2J_2=f_{010}\tilde{A} , \tag{10}$$
$$f_{111}\tilde{A}=3J_1+3J_2=f_{11\bar{1}}\tilde{A} .$$

Vertices V_i with energies $e_i (i=1,\ldots,6)$ correspond locally to facets, V_1 to $(11\bar{1})$, V_2 to (111), V_3 to (100), V_4 to (010), and V_5 and V_6 to (110). It is convenient to measure energies from the (110) energy. Then,

$$(f_{100}-f_{110})\tilde{A}=J_1 ,$$
$$(f_{111}-f_{110})\tilde{A}=J_2 . \tag{11}$$

The vertex energies e_i (for $\vec{\eta}=\vec{0}$) appearing in Fig. 2 are just the results of Eq. (11) with an irrelevant, but convenient for correspondence with the six-vertex model, constant J_1-J_2 added. The field terms in Fig. 2 serve then to provide the following correspondence between the total vertex energies $\tilde{e}_i$ and the energies e_i of the figure

$$\tilde{e}_i=f_{110}\tilde{A}+J_2-J_1+e_i . \tag{12}$$

The Andreev free energy $\tilde{f}(\vec{\eta},T)$ is then given in the model by

$$\tilde{f}(\vec{\eta},T)=f_{110}+\frac{J_2-J_1}{\tilde{A}}+f_{6V}(J_1,J_2,\mathscr{H},\mathscr{V},T) , \tag{13}$$

where $f_{6V}(e_i,\mathscr{H},\mathscr{V},T)$ is the six-vertex model free energy at temperature T with vertices e_i and the result, Eq. (9), connecting $\mathscr{H}$ and $\mathscr{V}$ to $\vec{\eta}$. Via Eq. (4), plots of Eq. (13) give the crystal shape near the (110) direction.

Note that the model of Fig. 2 describes a crystal surface which can vary from the [110] direction to the [100], [010], [111], and $[11\bar{1}]$ directions, but no further. This in effect limits the strict applicability of the model to directions near [110]. The (100), (010), (111), and $(11\bar{1})$ facets appear, but their lack of all relevant excitations pushes their roughening temperatures to infinity, as we shall see in detail in the following section. The specific six-vertex model results which we utilize are collected together in the Appendix.

Application of the same procedure at the (001) (or any equivalent) face is depicted in Fig. 3. The local vertex-facet correspondence is V_1 to (111), V_2 to $(\bar{1}\,\bar{1}\,1)$, V_3 to $(1\bar{1}1)$, V_4 to $(\bar{1}11)$, and V_5 and V_6 to (001). The equations corresponding to Eqs. (9)–(11) are readily found to be

$$\mathscr{H}=-\frac{A}{\sqrt{2}}(\eta_x+\eta_y) ,$$
$$\mathscr{V}=-\frac{A}{\sqrt{2}}(\eta_x-\eta_y) , \tag{14}$$

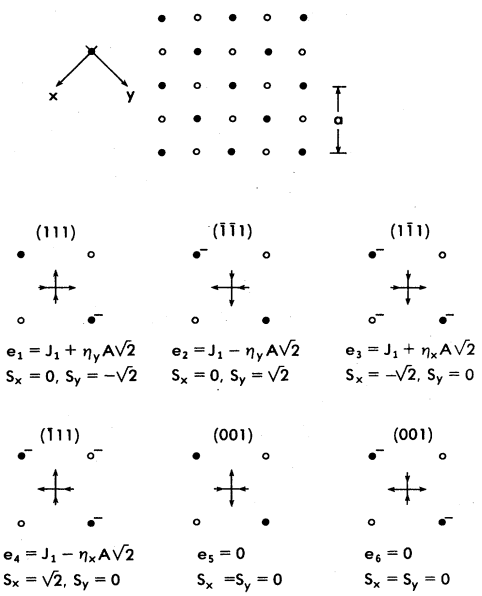

FIG. 3. Mapping of the six-vertex model onto the (001) face of an fcc crystal. See Sec. IV for notation.

where $A=a^2/4$,

$$f_{001}A=2J_1+J_2 ,$$
$$f_{111}A=3J_1+3J_2 , \tag{15}$$

and

$$(f_{111}-f_{001})A=J_1+2J_2 . \tag{16}$$

In this case the model does not actually include J_2 (see Fig. 3). However, J_2, which we shall always assume small, has only minor quantitative effects near the [001] direction, and we shall neglect it. In this case the analogs to Eqs. (12) and (13) become

$$\tilde{e}_i=f_{001}A+e_i \tag{17}$$

and

$$\tilde{f}(\vec{\eta},T)=f_{001}+f_{6V}(J_1,\mathscr{H},\mathscr{V},T) , \tag{18}$$

with $\mathscr{H}$ and $\mathscr{V}$ given by Eq. (14). From Eq. (4), a plot of Eq. (18) gives the ECS near the $\langle 001\rangle$ (equivalent) directions.

V. THERMAL EVOLUTION OF THE fcc SHAPE

In this section we present a detailed discussion of our results for the thermal evolution of the fcc crystal shape. Three cases will be considered: $J_2=0$, $J_2<0$, and $J_2>0$. Detailed descriptions of the thermal evolution will be given from the perspective of views along the [001] and [110] crystalline axes. Phase diagrams corresponding to T-x and T-y cuts of the crystal shape are also provided. All results here exploit the exact solution of the six-vertex model,[15–17] relevant details of which are relegated to the Appendix.

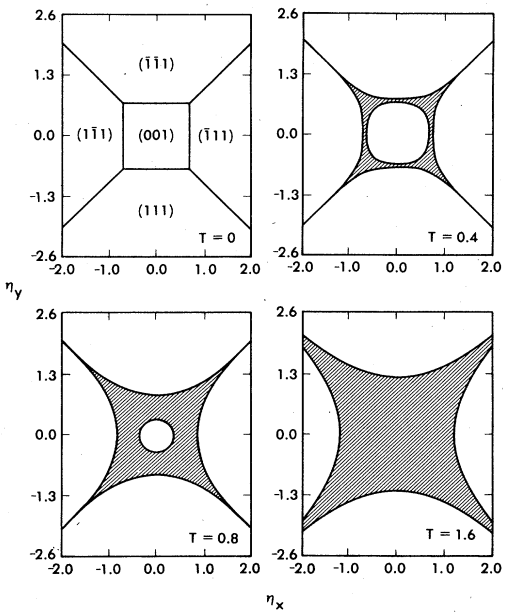

FIG. 4. Thermal evolution of the fcc crystal shape, viewed along the [001] axis, for $J_2=0$. Hatched areas are rounded (rough). Slopes are continuous across lines (Pokrovsky-Talapov phase boundaries) separating hatched areas from facets. The central (001) facet decreases in size with increasing T and vanishes at its roughening temperature $T=T_R=1.44J_1$. The facet designations at $T=0$ hold throughout.

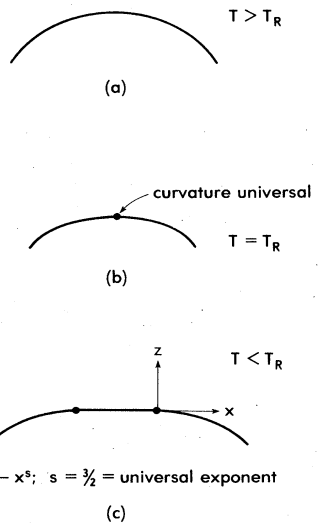

FIG. 5. Thermal evolution of a part of a crystal profile. The facet disappears at the roughening temperature T_R.

A. $R=0$

For the $R=0$ case, the equilibrium shape at $T=0$ consists of only the (100) and (111) facets and their symmetry equivalents as displayed in Fig. 1(a). We view the crystal first along the [001] direction and project it onto the plane. The $T=0$ shape is shown in Fig. 4 and one sees the square (001) facet and the adjoining facets. The edge between (111) and (001) and the other corresponding edges are highly degenerate. As soon as T is nonzero, there appear curved interfaces between the different facets shown crosshatched in Fig. 4. As the temperature is raised the (001) facet shrinks in size; the corresponding curved regions increase. Observe also that the facet becomes circular as $T\rightarrow T_R$. In fact, this occurs already at $T\sim T_R/2$. The last figure in the sequence of Fig. 4 displays the shape at $T>T_R((100))=1.443J_1$. Now the facet has disappeared entirely. The universal features associated with this transition were reported earlier[5,6] using both general duality arguments and model calculations like those described here. In the following paragraph we recapitulate the results briefly.

In Fig. 5 we sketch the temperature dependence of part of a crystal profile containing a facet. As T is raised, the facet shrinks in size and disappears altogether at $T=T_R$. At T_R the geometric mean (Gaussian) curvature, at the point where the facet has vanished, is given by[22]

$$(\kappa_1\kappa_2)^{1/2}=\frac{2}{\pi}\frac{d^2}{k_BT_R}\left[\frac{P_s-P_l}{2}\right], \tag{19}$$

where κ_1 and κ_2 are the principal curvatures and d is the microscopic height (a distance between crystal planes) of steps on that crystal surface which was flat at $T<T_R$. This result is expected to be universal[23] (independent of the particular crystalline substance) as it is a consequence of a continuous phase transition at which the correlation length diverges. A well-known analog of the result (19) is the universal jump in superfluid areal density at superfluid onset in ^{4}He films; [24] the XY model describing the transition in ^{4}He films is dual[25] to SOS models exhibiting roughening. Near but below T_R the linear size L of the facet has the temperature dependence[5,6]

$$L\sim ae^{c/\sqrt{t}}, \tag{20}$$

thus exhibiting an essential singularity. Here a is an interatomic distance and $t\equiv|T_R-T|/T_R$.

Further, the way the curved and faceted regions join is characterized by a universal shape exponent. Let $z(x,y)$ denote, as in Sec. III, the height of the crystal surface from the reference plane [the (001) plane in this case] with coordinates x and y. Figure 5(c) shows the shape along the direction x. $z(x)$ is a constant for $\lambda x<\eta_0$ and is curved for $\lambda x>\eta_0$. The shape exponent s is defined by

$$z(x)\sim(|\lambda x|-\eta_0)^s. \tag{21}$$

Within our model s turns out to be $\frac{3}{2}$, in contrast to the mean-field value of 2.[14] This exponent is universal and describes the crystal shape in all directions near the facet edge, reflecting the underlying Pokrovsky-Talapov transition[7,8] in $\tilde{f}(\bar{\eta})$. Rottman *et al.*[9] have observed $s=1.60\pm0.15$ in some samples of Pb films; we refer to their work in more detail in the following section.

Now consider the same crystal shown in Fig. 1(a), viewed along the [110] direction and projected onto the corresponding plane. The $T=0$ shape consists of straight edges, as seen in Fig. 6. When the temperature is nonzero, the degeneracy of the edges between the facets at $T=0$

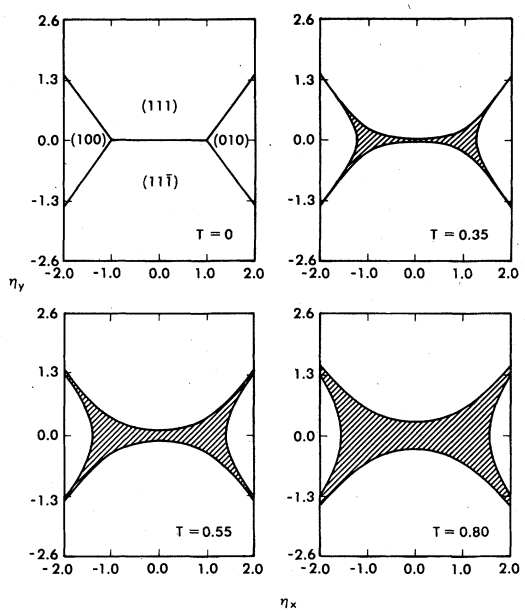

FIG. 6. Thermal evolution of the fcc crystal shape, viewed along the [110] axis, for $J_2=0$. Hatched areas are rounded (rough). Slopes are continuous across lines (Pokrovsky-Talapov phase boundaries) separating hatched areas from facets. The facet designations at $T=0$ hold throughout.

lead immediately to the appearance of rough (curved) surfaces (shown by crosshatching) between all the facets. As the temperature is raised, the curved regions increase in area while the facets shrink in size. The curved and faceted regions meet with a shape exponent of $\frac{3}{2}$ as described earlier. As the temperature is increased the facets shrink and disappear eventually by a roughening transition. In our model the (111) and (11$\bar{1}$) facets do not roughen; this is due to the solid-on-solid constraint which excludes relevant excitations. The phase diagram in the (η_y,T) plane is shown in Fig. 7. Figures 7(a) and 7(b) correspond to (η_y,T) projections of the crystal-shape evolution as viewed along the [100] and [110] directions. In Fig. 7(a) the (001) facet has a finite T_R, and along a fixed $0<T<T_R$ cut, as η_y is varied, one passes from the (111) facet onto a curved (rough) region, from the curved region onto the (001) facet, from this facet onto another curved region, and finally onto the ($\bar{1}\bar{1}1$) facet. All crossings from facets to curved regions are via Pokrovsky-Talapov transitions, indicated by the solid lines. The shape of the phase diagram around T_R reflects the essential singularity described earlier. One expects $T_R((111))$ and $T_R((\bar{1}\bar{1}1))$ to be greater than $T_R((001))$ and so the restricted cut sketched in Fig. 7(a) is fairly accurate. A simple estimate of $T_R((111))$ follows from comparing $T=0$ step energies for the (001) and (111) facets. Since the $T=0$ step energy for the (111) facet is twice that of the (001) facet, we expect that $T_R((111))\sim 2T_R((001))$. In Fig. 7(b), in contrast, the edge between (11$\bar{1}$) and (111) roughens immediately.

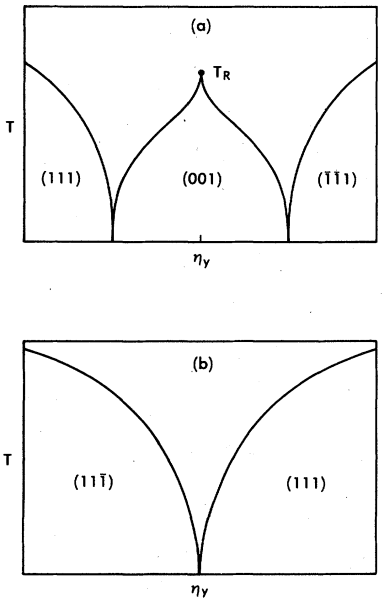

FIG. 7. T-η_y or, equivalently, the T-y phase diagrams for the fcc crystal when $J_2=0$ for (a) the mapping onto the [001] direction and (b) the mapping onto the [110] direction. Solid lines indicate Pokrovsky-Talapov transitions (boundaries between facets and rough surfaces).

These results for $R=0$ complement our earlier work,[5,6] providing a more global description of the crystal shapes. They are essentially in agreement with the results of Rottman and Wortis,[1,2] who discussed a simple cubic lattice and used mean-field theory supplemented by general considerations regarding fluctuations in two-dimensional interfaces. In fact, apart from the unfortunate feature that we cannot explicitly treat roughening of (111) facets, our work provides a qualitatively correct and unified description with *exact* results for critical properties.

B. $R<0$

Several new features appear for $R<0$. Our results differ somewhat from those of Rottman and Wortis[1,2] and we discuss the differences in this section. As noted earlier the change in sign of R removes the degeneracy along the edge between [111] and [11$\bar{1}$] directions and the $T=0$ global shape is shown in Fig. 1(a). For $J_1=1.0$, $J_2=-0.1$, a cross section projected onto a plane is shown in Fig. 8. The phase diagram and the thermal evolution are again obtained using the six-vertex model results. The $R<0$ situation corresponds to a ferroelectric model which exhibits unusual properties. The crucial feature which makes the shape and the nature of the transitions interesting is that the edge between the (111) and (11$\bar{1}$) facets does *not* roughen as the temperature is raised above zero! This is seen in Fig. 8 where a curved surface interjects itself between the pair (111) and (100) and their equivalents while in contrast the edge between (111) (11$\bar{1}$) persists as the temperature is raised. The former, of course, was to be expected from the zero-temperature degeneracy of the (100)-(111) edge. The transition between the (100) facets and the rough interface is of the Pokrovsky-Talapov type as is the transition between (111) facets and the rough interface. As there is no proof of this fact, we have provided one within the six-vertex model in the Appendix. Thus there exists a first-order transition between the (111) and

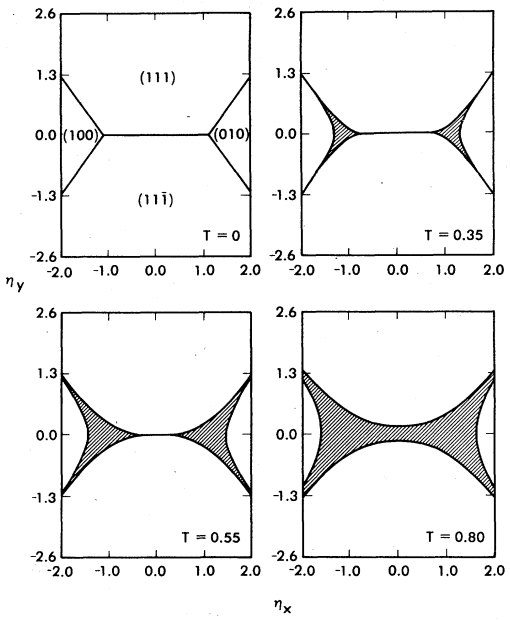

FIG. 8. Thermal evolution of the fcc crystal shape, viewed along the [110] axis, for $J_2/J_1=-0.1$. Hatched areas are rounded (rough). The line separating the (111) and (11$\bar{1}$) facets is a sharp edge (first-order phase boundary) whose length decreases with increasing T until it vanishes at $T=T_c\approx 0.6J_1$. Slopes are continuous across lines (Pokrovsky-Talapov phase boundaries) separating hatched areas from facets. The facet designations at $T=0$ hold throughout.

(11$\bar{1}$) facets which persists up to a finite temperature $T_c\approx 0.6J_1$.

As T is increased from zero, the length of the edge decreases until at T_c it disappears. Above this temperature a smoothly rounded interface appears between the two facets as shown in Fig. 8. Also, we expect that at temperatures above T_c, the (100), (111), etc., facets will roughen with the universal behavior described earlier, a phenomenon not present in our mapping for the (110) face.

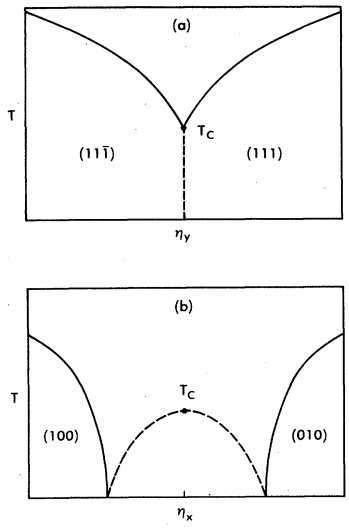

FIG. 9. (a) T-η_y (or T-y) and (b) the T-η_x (or T-x) phase diagrams for the fcc crystal for the mapping onto the [110] direction. Here $J_2/J_1=-0.1$. Solid lines indicate Pokrovsky-Talapov transitions (boundaries between facets and rough surfaces), and dotted lines are first-order phase boundaries associated with the edge separating the (111) and (11$\bar{1}$) facets (see Sec. V B).

There are several new and interesting features associated with the $R<0$ case. Refer to Fig. 9(a), where a T-η_y cut of the phase diagram (crystal shape) is given. Pokrovsky-Talapov lines are shown (solid lines) as is the first-order edge transition (dotted line) between the (11$\bar{1}$) and (111) facets. As one approaches T_c vertically from above the curvature, $\kappa_y(y=0)$ of the crystal in the horizontal direction approaches infinity in order that the (11$\bar{1}$)-(111) edge be smoothly formed as a function of T. The explicit form of this singularity is[26]

$$\kappa_y(y=0)=\alpha/(T-T_c)\ . \tag{22}$$

Because the Pokrovsky-Talapov correlation lengths diverge as $T\rightarrow T_c^+$, we believe this temperature dependence to be universal. The surface stiffness

$$\Gamma_y=\left.\frac{\partial^2 f(\vec{s})}{\partial s_y^2}\right|_{s_y=0}=\frac{1}{\kappa_y}$$

then approaches zero as $(T-T_c)$.

A cut in the T-η_x plane, shown in Fig. 9(b), is even more interesting. Based on arguments given in the Appendix (arguments which are very plausible, but not entirely rigorous), the dotted line in Fig. 9(b), which traces the ends of the (11$\bar{1}$)-(111) edge is a line of first-order transitions. The transition at T_c in the six-vertex model is rigorously first order and exhibits a latent heat as $T\rightarrow T_c^+$ at $\eta=0$. In the crystal-shape problem this latent heat becomes a discontinuous jump in $[\partial z(\vec{x})/\partial T]_{\vec{x}=\vec{0}}$. The analog of this jump as the dotted line is approached, from either rough region outside the inverted, dotted "parabola," at any $T<T_c$, is a discontinuity in the slope s_x. The curvature in the y direction at $\eta_x=0$ $(=-\lambda x)$ should, by analogy to Eq. (22), then diverge as $1/|x-x_c|$, where x_c is the position of either end of the (11$\bar{1}$)-(111) edge.

The mean-field theory of Rottman and Wortis[1,2] for a simple-cubic lattice with repulsive second-neighbor interaction produces a slope discontinuity all around the perimeter of certain facets in certain temperature ranges. These discontinuities decrease in magnitude and vanish at tricritical points as the temperature is raised. In contrast we find no slope discontinuities at facet perimeters but only at edge ends within the six-vertex model picture. The reasons for this difference are not clearly understood. It could either be due to the neglect of overhangs and bubbles in our model or be due to the limitations of mean-field theory.

C. $R>0$

We conclude with a discussion of the $R>0$ case. The limitations of the SOS type of models describing global features are apparent. Because of the lack of relevant excitations, the $T=0$ shape is not described completely from the [001] direction. However, if we focus on the

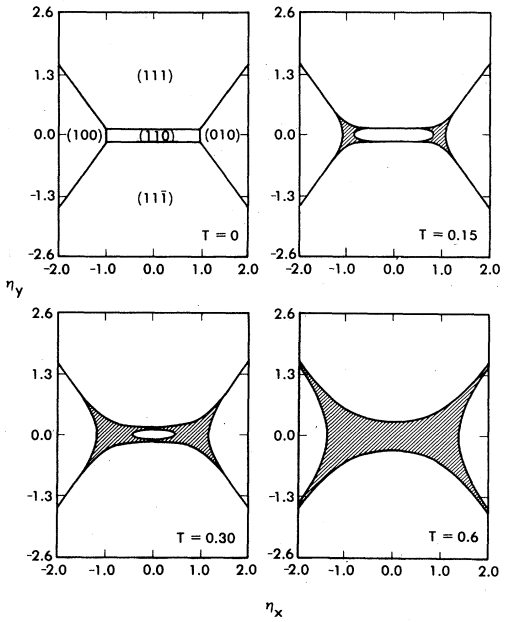

FIG. 10. Thermal evolution of the fcc crystal shape, viewed along the [110] axis, for $J_2/J_1=0.1$. Hatched areas are rounded (rough). Slopes are continuous across lines (Pokrovsky-Talapov phase boundaries) separating hatched areas from facets. The central (110) facet decreases in size with increasing T and vanishes at its roughening temperature $T=T_R\approx 0.5J_1$. The facet designations at $T=0$ hold throughout.

(110) facet a good local description can be obtained as before. Recall that in contrast to the $R=0$ case (see Fig. 1) the next-nearest-neighbor interactions have lifted the degeneracy of the edge between [111] and [11$\bar{1}$] directions, causing the appearance of a rectangular (110) facet at $T=0$ between the (111), (100), (010), and (11$\bar{1}$) facets. The $T=0$ view of the equilibrium crystal shape along the [110] direction is shown in Fig. 10. At $T>0$, rough surfaces appear between the (100) and (111) and the (100) and (110) pairs. The facet shape is elliptical as shown for $T=0.15$ in Fig. 10. As the temperature is raised the facet shrinks in size (at $T=0.30$ in Fig. 10) and disappears altogether for $T>T_R((110))\approx 0.5J_1$ (see the $T=0.6$ picture in Fig. 10). All the universal features described for the $R=0$ case are found here within the exact calculations. The corresponding (η_y,T) phase diagram is sketched in Fig. 11. Finally, we note again that we do not have an exactly solvable model for viewing the crystal along the [111] direction or an appropriate model for the [001] direction when $J_2<0$. These would indeed be interesting to find.

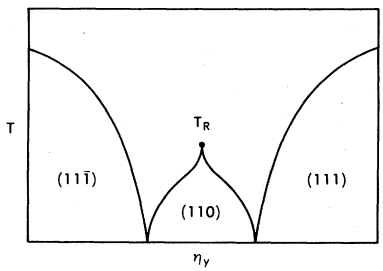

FIG. 11. T-η_y (or T-y) phase diagram for the mapping onto the [110] direction with $J_2/J_1=0.1$. Solid lines indicate Pokrovsky-Talapov transitions (boundaries between facets and rough surfaces).

VI. ON MEASUREMENTS OF UNIVERSAL EXPONENTS

In this section we make a few remarks on experiments designed to measure universal crystal-shape features. We provide crude estimates of some of the limitations on the range of applicability of theoretical predictions. These include scaling corrections to the leading critical behavior, elastic effects (which are of order $1/\mathscr{R}$ where $\mathscr{R}$ is the size of the crystal), corrections to the surface tension due to curvature (also of order $1/\mathscr{R}$), and finite-size effects.

Consider a profile of a crystal surface with a z-x coordinate system, the origin at the center of the facet (see Fig. 5). The free energy $f(s)$ has the following expansion in the slope s (see Refs. 5, 15, and the Appendix):

$$f=f_0+\eta_0|s|+\frac{b}{3}|s|^3+\frac{cs^4}{4}+\cdots . \tag{23}$$

Performing the Legendre transformation, in the manner of Andreev, one has

$$\tilde{f}(\eta)=f_0-\frac{2b}{3}\left[\frac{\eta-\eta_0}{b}\right]^{3/2}+\frac{c}{4}\left[\frac{\eta-\eta_0}{b}\right]^2+\cdots ,\quad \eta>\eta_0 ,$$
$$=f_0,\quad \eta<\eta_0 . \tag{24}$$

The profile shape is then given by

$$z(x)=z_0\left[1-\frac{2}{3}\left[\frac{f_0}{b}\right]^{1/2}\left[\frac{x-x_0}{z_0}\right]^{3/2}+\frac{cf_0}{4b^2}\left[\frac{x-x_0}{z_0}\right]^2+\cdots\right], \tag{25}$$

where $z_0=f_0/\lambda$ is the distance of the center of the facet from the center of the crystal and $x_0=\eta_0/\lambda$ is the distance from the edge to the center of the facet.

The scaling of the coefficients in the expansion of Eq. (24) near the roughening transition T_R can be deduced easily. If ξ_R is the correlation length near but below T_R we expect $f-f_0\sim\xi_R^{-2}$ and the slope $s=\partial z/\partial x\sim\xi_R^{-1}$. This yields $\eta_0\sim\xi_R^{-1}$ and $b\sim\xi_R$ which agree with known results for the six-vertex model. We can also deduce that $c\sim\xi_R^2$ which has not been derived explicitly with any model. We may thus write

$$b=f_0\left[\frac{4}{9\alpha_1^2}\right]\frac{\xi_R}{a},\quad \frac{c}{4b^2}=\frac{\alpha_2}{2f_0} , \tag{26}$$

where α_1 and α_2 have weak temperature dependences, and a is a microscopic length. Inserting Eq. (26) in Eq. (25) produces

$$z(x)=z_0\left[1-\alpha_1\left[\frac{a}{\xi_R}\right]^{1/2}\left[\frac{x-x_0}{z_0}\right]^{3/2}+\frac{\alpha_2}{2}\left[\frac{x-x_0}{z_0}\right]^{2}+\cdots\right]. \tag{27}$$

Suppose T is not near T_R so that $\xi_R\sim a$. Let

$$\alpha_1(a/\xi_R)^{1/2}\equiv\tilde{\alpha}_1 . \tag{28}$$

Then

$$\frac{z-z_0}{z_0}=-\left[\frac{x-x_0}{z_0}\right]^{3/2}\left[\tilde{\alpha}_1-\frac{\alpha_2}{2}\left[\frac{x-x_0}{z_0}\right]^{1/2}\right]. \tag{29}$$

The Pokrovsky-Talapov (PT) exponent $\frac{3}{2}$ in Eq. (27) will be inapplicable when

$$[(x-x_0)/z_0]^{1/2}\gtrsim 1 . \tag{30}$$

The measurement of the PT exponent for small lead crystals reported recently by Rottman *et al.*[9] show corrections roughly when $[(x-x_0)/z_0]^{1/2}\sim 0.3$, in agreement with Eq. (30). This discussion is certainly valid within our model and gives a reasonable order-of-magnitude estimate for the critical region. However, other forms of the correction term cannot be ruled out.

We note parenthetically that Eq. (30) can be understood from scaling arguments. The transverse correlation length $\xi_\perp$ (roughly the mean distance between steps on the surface) at fixed T behaves as $\xi_\perp\sim(\eta-\eta_0)^{-1/2}$, i.e., $\nu_\perp=\frac{1}{2}$ at the PT transition.[27] In terms of crystal-shape parameters this becomes $(\xi_\perp/a)\sim[z_0/(x-x_0)]^{1/2}$ and Eq. (30) translates to $a/\xi_\perp>1$ which is what one might expect.

Now we turn to possible finite-size corrections to the PT transition (i.e., of order $1/\mathscr{R}$ where $\mathscr{R}$ is the size of the crystal) due to the effects of elasticity. As argued by Herring,[28] these will produce corrections to the surface free-energy density of order $f_0(a/z_0)$. If this is to be less than the PT term in Eq. (24), we easily obtain the condition

$$x-x_0>(a^2z_0)^{1/3} , \tag{31}$$

in order-of-magnitude agreement with the observations of Rottman *et al.*[9] on lead crystals. Equation (31) can again be derived from scaling arguments. The critical part of the surface free-energy density varies as

$$f_0a^2\xi_{||}^{-1}\xi_\perp^{-1}\sim f_0[(x-x_0)/z_0]^{3/2} ,$$

noting that the correlation length $\xi_{||}$ parallel to steps on the surface has exponent 1 (Ref. 27) and recalling from above that $\xi_\perp$ has exponent $\frac{1}{2}$. The requirement that $f_0a^2\xi_{||}^{-1}\xi_\perp^{-1}$ dominate the elastic energy $f_0(a/z_0)$ yields Eq. (31).

There are several other possible sources of $O(1/\mathscr{R})$ corrections. One is due to the dependence of surface tension on curvature.[29] A second is due to the fact that the thermodynamic limit is not taken in a finite system, leading to effects proportional to the perimeter of a facet and hence of $O(1/\mathscr{R})$. Both of these sources may be expected to produce corrections at most of the order of that given by Eq. (31). Finally, finite-size corrections to scaling can produce corrections to the second term in Eq. (24) measured by the ratio of a correlation length to a characteristic dimension of the finite crystal. The possible characteristic dimensions are the size of the crystal ($\sim z_0$), the size of a facet ($\sim z_0$ for $T\ll T_R$), and the radius of curvature near a facet edge ($\sim z_0[(x-x_0)/z_0]^{1/2}$ from Eq. (24)). Comparing the ratios of $\xi_{||}$ and $\xi_\perp$ to these yields conditions no more stringent than that of Eq. (31).

We summarize our conclusions regarding observations of the PT transition away from T_R as follows. The PT exponent of $\frac{3}{2}$ can be expected to be observable within a window near the facet edge. The window is bounded above by a noncritical correction important when $\xi_\perp/a$ becomes too small; see Eq. (30). Note that the correction is of the mean-field form[14] in that its exponent is 2. The window is bounded below by finite-size effects due to elastic strain or the other $O(1/\mathscr{R})$ effects. The specific condition is given by Eq. (31). The uncertainty in determining x_0 precisely (this is the analog of the difficulty in pinning T_c down in ordinary critical phenomena) from pictures of the shape is an important source of error.

We now return to the case T near T_R. Using Eq. (27) one finds that the condition for the corrections to the leading critical behavior to be small is

$$\left[\frac{\xi_R}{a}\right]^{1/2}\left[\frac{x-x_0}{z_0}\right]^{1/2}\lesssim 1 . \tag{32}$$

This can be rewritten as

$$\left[\frac{\xi_R}{\xi_{||}}\right]^{1/2}\lesssim 1 . \tag{33}$$

Since

$$\xi_R\sim ae^{c/\sqrt{t}} , \tag{34}$$

where $t\equiv|T_R-T|/T_R$, the PT critical region shrinks rapidly as $T\to T_R$. Elastic effects also become important when

$$x-x_0>(a^2z_0)^{1/3}\left[\frac{\xi_R}{a}\right]^{1/3} , \tag{35}$$

in contrast to Eq. (31).

In order to be able to observe a facet the facet size L_f must be larger than ξ_R, otherwise the facet appears rough and hence rounded. This implies $\xi_R\ll L_f\sim x_0\sim x_0(a/\xi_R)$, which yields

$$z_0a>\xi_R^2 , \tag{36}$$

or, using Eq. (34),

$$z_0/a>e^{2c/\sqrt{t}} . \tag{37}$$

It is worth noting that if $c=1$ and $t=10^{-1}$, this condition is $z_0>5\times10^2a\sim10^{-5}$ cm, while for $t\sim10^{-2}$ it becomes $z_0>5\times10^8a\sim5$ cm. The accessible critical region

is narrow in t. Within the six-vertex model $c=\pi^2/4\sqrt{2}\ln 2=2.1$ and the situation is worse. Fortunately, c is not universal. For ^{4}He films the analogous quantity lies in the range $c\simeq 0.9$–1.4.[24,30]

For $T>T_R$ the second term in Eq. (27) vanishes as does x_0, giving[31]

$$z(x)=z_0\left[1-\frac{\gamma}{2}\left[\frac{x}{z_0}\right]^2+\cdots\right]. \tag{38}$$

For $T\to T_R$ [assuming equal principal curvatures; see Eq. (19)], γ is related to the universal curvature κ by

$$\gamma(T_R)=z_0\kappa(T_R)=\frac{2}{\pi}\frac{f_0 d^2}{k_B T_R}. \tag{39}$$

There are nonanalytic corrections to Eq. (38);[32] these will be unimportant for $(x/z_0)\ll 1$. Elastic effects will cease to be important for

$$x>(z_0 a)^{1/2}, \tag{40}$$

again assuming an elastic surface energy density $\sim f_0(a/z_0)$. For lead crystals with $z_0\sim 10^{-3}$ cm, this becomes $x>10^{-5}$ cm, an observable effect.

Finally, we remark on the temperature dependence of the crystal surface curvature for $T>T_R$. This will be of the form[33]

$$\kappa(T)=\kappa(T_R)\left[1+\frac{2\pi}{c}\left[\frac{T-T_R}{T_R}\right]^{1/2}+O\left[\frac{T-T_R}{T_R}\right]\right], \tag{41}$$

where c is the same constant appearing in the correlation length ξ_R [see Eq. (34)].

VII. DISCUSSION AND SUMMARY

We have presented a global description of the thermal evolution of the equilibrium shape of an fcc crystal including both first- and second-nearest-neighbor interactions. The description for $T>0$ was, of necessity, somewhat piecemeal in that the solid-on-solid model had to be applied separately along different directions in the crystal. This drawback is balanced by the benefit of obtaining exact results in critical regions. An outstanding problem is the construction of a tractable model which deals both globally with the crystal shape and yet retains exact descriptions of critical phenomena such as roughening and Pokrovsky-Talapov transitions.

The overall picture presented here has, as noted earlier, received substantial experimental support from the experiments on lead[9] and helium[10] crystals. Our model provides no mechanism for a facet and an adjoining rough surface to be separated by a line across which the crystal slope is discontinuous. Such a feature appears in the mean-field theory of Rottman and Wortis,[1,2] as discussed above, and has been seen in small gold crystals.[34] It is not, however totally clear that the crystals were in equilibrium.[2] Further, there is evidence[35] that slope discontinuities at facet edges can only appear in solid-on-solid models when there are long-ranged attractive[36] forces between steps, a situation not relevant to gold. One possibility is that the action of voids and overhangs produces a first-order transition mirrored by the slope discontinuity in the shapes. Another is that the slope discontinuities seen in mean-field theory are artifacts of the approximations made. The question remains open.

Concerning the possibility of observing sharp edges on equilibrium shapes, we note that elastic strain effects are believed[37] to render impossible atomically sharp edges. The extent of the consequent rounding has not yet been estimated. Finally, we note that the general features found here for the thermal evolution of the fcc crystal shape are expected (subject to limitations of SOS models) to be valid for other lattices.

ACKNOWLEDGMENTS

We wish to thank Michael Wortis, Craig Rottman, Steve Teitel, and David Edwards for useful conversations concerning this work. One of us (C.J.) wishes to thank the Alfred P. Sloan Foundation and the National Science Foundation for support.

APPENDIX

Explicit analytic expressions for the phase boundaries of Figs. 4, 6, 8, and 10 can be found in the paper by Lieb and Wu.[15] We will rederive their expressions below as part of an extension of their work allowing explicit determination of the nature of the phase transitions for general η_x and η_y. It seems advantageous to first give the results used in plotting the curves for the figures.

After making the variable change from the six-vertex fields $(\mathscr{H},\mathscr{V})$ to the fields (η_x,η_y) (see Sec. IV), the four outer phase boundaries (excluding any central facet) for Figs. 6, 8, and 10 are (letting the unit cell areas A and $\tilde{A}$ of Sec. IV be unity for convenience)

$$\frac{\eta_y}{\sqrt{2}}=J_1-J_2-k_B T \times\ln\{\cosh(\beta\eta_x)+[\sinh^2(\beta\eta_x)+e^{2\beta J_1}]^{1/2}\} \tag{A1}$$

for the lower boundaries. Equation (A1) holds only for $\eta_y\le 0$. To obtain the equation for the upper boundaries let $\eta_y\to-\eta_y$ in Eq. (A1) and use the restriction $\eta_y\ge 0$. For the right-hand-side boundaries we have

$$\eta_x=J_1-J_2+k_B T \times\ln\left\{\cosh\left[\frac{\beta\eta_y}{\sqrt{2}}\right]+\left[\sinh^2\left[\frac{\beta\eta_y}{\sqrt{2}}\right]+e^{2\beta J_2}\right]^{1/2}\right\}, \tag{A2}$$

the left-hand-side boundaries being found from Eq. (A2) by the replacement $\eta_x\to-\eta_x$. The four outer boundaries for Fig. 4 are given by Eqs. (A1) and (A2) with the replacements $\eta_x\to\eta_x/\sqrt{2}$ and $\eta_y\to 2\eta_y$, as can be seen by comparing Eqs. (9) and (16) of the text. In addition to these boundaries, when $\eta_y=0$ in Eq. (A1) it occurs at symmetric points on the η_x axis. We connect these two points to give the first-order phase boundary for the edge

separating facets [i.e., the (111) and (11$\bar{1}$) facets of Fig. 8]. The boundary for the central facet in Fig. 10 is given by

$$\eta_x=\Sigma(\lambda-\theta_0+s)+\Sigma(s)\ ,$$
$$\eta_y=-[\Sigma(\lambda-\theta_0+s)-\Sigma(s)]\sqrt{2}\ , \tag{A3}$$

where s is varied through the range $-2\lambda\le s\le 2\lambda$ and

$$\lambda=\ln[\,|\Delta|+(\Delta^2-1)^{1/2}]\ ,$$
$$\theta_0=\ln[(1+\eta e^{\lambda})/(e^{\lambda}+\eta)]\ , \tag{A4a}$$

where

$$\eta=e^{\beta(J_1-J_2)}\ ,$$
$$\Delta=\cosh[\beta(J_1-J_2)]-\tfrac{1}{2}e^{\beta(J_1+J_2)}\ . \tag{A4b}$$

The function $\Sigma(\phi)$ is defined by[15]

$$\Sigma(\phi)=\ln\frac{\cosh[\frac{1}{2}(\lambda+\phi)]}{\cosh[\frac{1}{2}(\lambda-\phi)]}$$
$$-\frac{\phi}{2}-\sum_{n=1}^{\infty}\frac{(-1)^n e^{-2n\lambda}\sinh(n\phi)}{n\cosh(n\lambda)}\ ,\quad |\phi|<3\lambda\ . \tag{A5}$$

The results of Eqs. (A3) and (A4) are found in the original work of Sutherland, Yang, and Yang.[16] The roughening transition is at $\Delta=-1$, $\vec{\eta}=\vec{0}$, conditions determining T_R. For the (001) facet of Fig. 4, one uses Eqs. (A3)–(A5) with the replacements $\eta_x\to\sqrt{2}\eta_x$ and $\eta_y\to 2\eta_y$.

Precise data for Figs. 7, 9, and 11 can, of course, be extracted from Eqs. (A1)–(A5); we have contented ourselves with sketches. The temperature T_c is determined from the condition $\Delta=+1$.[15,16]

Near but below T_R (roughly for $0.8\le T/T_R\le 1$) the (001) facet is circular with radius R given by[5,15]

$$R=\frac{4\sqrt{2}k_BT}{(P_s-P_l)A}e^{-\pi^2/4(2t\ln 2)^{1/2}}=\frac{k_bTa}{A(P_s-P_l)}\xi_R^{-1}\ , \tag{A6}$$

where ξ_R is the correlation length for the roughening transition (see Sec. VI). In the same temperature regime the free energy $f(s)$ possesses the expansion[5,15]

$$f(\vec{s})=f_0+\eta_0|\vec{s}|+\frac{b|\vec{s}|^3}{3}+O(\vec{s}^{\,4})\ , \tag{A7}$$

where the step free energy $\eta_0=R(P_s-P_l)$ and the coefficient $b=\pi^2/16\eta_0$. The $s=0$ free energy f_0 is given explicitly in Refs. 15 and 16.

We next turn to our explicit proof that the outer boundaries of Figs. 4, 6, 8, and 10 are boundaries for Pokrovsky-Talapov transitions. We use the standard six-vertex notation and variables.[15,16] Vertical and horizontal polarizations are y and x, and their conjugate electric fields are $\mathscr{V}$ and $\mathscr{H}$. Let $V=\beta\mathscr{V}$ and $H=\beta\mathscr{H}$. The zero-field vertices are characterized by energies (times β) of K_1 and K_2, related, for example, to our J_1 and J_2 by $K_1=\beta(J_1-J_2)$, $K_2=\beta J_1$ for the model applied to the [110] direction. From Refs. 15 and 16, if $f_{\mathscr{H},y}$ is the free energy per site obeying $df_{\mathscr{H},y}=-x\,d\mathscr{H}+\mathscr{V}\,dy$, then for $y\ge 0$ and $\mathscr{H}>K_1/2\beta_1$ conditions which restrict the study to near the boundary of the region where the system is frozen into vertex e_1 [i.e., the (11$\bar{1}$) facet],

$$-\beta f_{\mathscr{H},y}=-K_2+H+\int_C\ln[\lambda_R(p_0)]\rho(p_0)dp_0\ , \tag{A8}$$

where C is a particular curve in the complex plane and $\rho(p_0)dp_0$ is real, being a density of points. Using the facts that the curve C is symmetric under the transformation $p_0\leftrightarrow p_0^*$ and that $\rho(p_0)dp_0=\rho(-p_0^*)dp_0^*$, Eq. (A8) can be put in the form

$$-\beta f_{\mathscr{H},y}=-K_2+H$$
$$+\tfrac{1}{2}\int_C\ln[\lambda_R(p_0)\lambda_R(-p_0^*)]\rho(p_0)dp_0\ . \tag{A9}$$

Making a change of variables to the real variable f, where f is such that $df/dp_0=\rho(p_0)$ along C and $f=0$ at the midpoint of C, Eq. (A9) becomes

$$-\beta f_{\mathscr{H},y}=-K_2+H$$
$$+\tfrac{1}{2}\int_{-f_1}^{f_1}\ln[\lambda_R(p_0(f))\lambda_R(-p_0^*(f))]df\ , \tag{A10}$$

where[15,16] $f_1=(1-y)/4$. Now,

$$\lambda_R=\frac{2\Delta-\eta-e^{ip_0}}{1-\eta e^{ip_0}}\ , \tag{A11}$$

where

$$2\Delta=e^{K_1}+e^{-K_1}-e^{2K_2-K_1}\ ,$$
$$\eta=e^{K_1}\ , \tag{A12}$$

and we assume $K_1>0$. Some algebra using Eqs. (A10) and (A11) produces

$$-\beta f_{\mathscr{H},y}=-K_2+H+\tfrac{1}{2}\int_{-f_1}^{f_1}\ln\left[\frac{(2\Delta-\eta)^2-(2\Delta-\eta)(e^{ip_0}+e^{-ip_0^*})+e^{i(p_0-p_0^*)}}{1+\eta e^{2i(p_0-p_0^*)}-\eta(e^{ip_0}+e^{ip_0^*})}\right]df\ . \tag{A13}$$

The equation determining $p_0(f)$ is[15,16]

$$p_0(f)=-2iH+2\pi f-\int_{-f_1}^{f_1}\Theta(p_0(f),p_0(f'))df'\ , \tag{A14}$$

where

$$\Theta(p_0,q_0)=2\tan^{-1}\left[\frac{\Delta\sin[(p_0-q_0)/2]}{\cos[(p_0+q_0)/2]-\Delta\cos[(p_0-q_0)/2]}\right]\ . \tag{A15}$$

It is convenient to use the variable

$$p=p_0+2iH\ , \tag{A16}$$

so that Eq. (A14) becomes

$$p(f)=2\pi f-\int_{-f_1}^{f_1}\Theta(p(f)-2iH,p(f')-2iH)df'\ . \tag{A17}$$

For $4f_1=(1-y)\ll 1$, we assume, with Lieb and Wu,[15] that the only important p's are small. Then the function Θ simplifies, and Eq. (A17) reduces to

$$p=2\pi f-\Delta\int_{-f_1}^{f_1}\frac{p(f)-p(f')}{\cosh(2H)-\Delta}df'\ . \tag{A18}$$

This integral equation may be solved exactly, assuming $\cosh(2H)\neq\Delta$ [$\cosh(2H)=\Delta$ gives the $(11\bar{1})$-(111) edge ends]; one readily finds

$$p(f)=\frac{2\pi f}{1+\{(1-y)\Delta/2[\cosh(2H)-\Delta]\}}\ . \tag{A19}$$

Lowest order in $(1-y)$ is all that is required here, i.e.,

$$p(f)=2\pi f\ . \tag{A20}$$

Inserting this solution in Eq. (A13) produces

$$-\beta f_{\mathscr{H},y}=-K_2+H+\tfrac{1}{2}\int_{-f_1}^{f_1}\ln\left[\frac{(2\Delta-\eta)^2-2(2\Delta-\eta)\cos(2\pi f)+e^{4H}}{1+e^{4H}\eta^2-2\eta e^{2H}\cos(2\pi f)}\right]df\ . \tag{A21}$$

As $f_1=(1-y)/4\ll 1$, we may expand the integrand in Eq. (A21) to order f^2 and integrate. After some algebra the result may be put in the form

$$-\beta f_{\mathscr{H},y}=-K_2+H+\frac{1-y}{2}\ln\left[\frac{e^{2H}+\eta-2\Delta}{\eta e^{2H}-1}\right]+\frac{8\pi^2}{3}e^{2H}\left[\frac{1-y}{4}\right]^3\left[\frac{(\Delta-\eta)(1+\eta^2-2\eta\Delta)+\eta(e^{4H}-1)\{\eta\Delta-[(1+\eta^2)/2]\}}{(2\Delta-\eta-e^{2H})^2(1-\eta e^{2H})^2}\right]\ . \tag{A22}$$

We rewrite this as

$$f_{\mathscr{H},y}=\beta(K_2-H)+a(y-1)+b(y-1)^3\ . \tag{A23}$$

Making the Legendre transformation to $f_{\mathscr{H},\mathscr{V}}=f_{\mathscr{H},y}-y\mathscr{V}$, the minimum over y of which gives the equilibrium value of y, we find that $y=1$ for $\mathscr{V}\geq a$, or, using Eq. (A22)

$$e^{2V}\geq\frac{e^{2H}+\eta-2\Delta}{\eta e^{2H}-1}\ . \tag{A24}$$

In this case, $x=-(\partial f_{\mathscr{H},y}/\partial\mathscr{H})=1$ as well, and the system is frozen into vertex e_1. Transforming to the variables η_x and η_y of the text [Eq. (14)] reproduces Eq. (A1) for the $(11\bar{1})$ facet boundary, aside from any (111)-$(11\bar{1})$ edge. The form of Eq. (A23) (lacking a quadratic term but containing a cubic one) ensures that the transition at the boundary is Pokrovsky-Talapov. The analogous results for the other boundaries are derived in a similar fashion.

The argument that the dotted line in Fig. 9(b), tracing the ends of the $(11\bar{1})$-(111) edge as a function of T, is a line of first-order transitions goes as follows. The transition as the line is approached from above (T decreasing, $\vec{\eta}=\vec{0}$) is known[15] to be first order. It is first order because above T_c, the order parameter s_y is zero, while immediately below T_c, s_y must jump to ± 1 (in appropriate units) corresponding to the facets $(11\bar{1})$ and (111). This discontinuous jump in the order parameter signals a first-order transition. If we approach the dotted line at fixed T by varying η_x, once again a discontinuous jump in s_y must occur. Consequently, the whole dotted line is (very plausibly) a line of first-order transitions. Since it is a line of first-order transitions we then expect a discontinuous jump in s_x at the edge ends. The analog of this jump in s_x, when T_c is approached at $\vec{\eta}=\vec{0}$, is the known[15] jump in $[\partial f(\vec{\eta},T)/\partial T]_{\vec{\eta}=\vec{0}}$, which is just the latent heat at T_c for the ferroelectric transition in the original six-vertex model.

[1]C. Rottman and M. Wortis, Phys. Rev. B **29**, 328 (1984).
[2]C. Rottman and M. Wortis, Phys. Rep. **103**, 59 (1984). This paper reviews the field and gives many additional references.
[3]See, e.g., J. D. Weeks, in *Ordering in Strongly Fluctuating Condensed Matter Systems,* edited by T. Riste (Plenum, New York, 1980).
[4]W. K. Burton, N. Cabrera, and F. C. Frank, Philos. Trans. R. Soc. London, Ser. A **243**, 299 (1951). See also our Refs. 3, 5, 6, 8, and 20.
[5]C. Jayaprakash, W. F. Saam, and S. Teitel, Phys. Rev. Lett. **50**, 2017 (1983).
[6]W. F. Saam, C. Jayaprakash, and S. Teitel, in *Quantum Fluids*

and Solids—1983 (Sanibel Island, Florida), edited by E. D. Adams and G. G. Ihas, (A.I.P., New York, 1983), p. 371.

[7]V. L. Pokrovsky and A. L. Talapov, Phys. Rev. Lett. **42**, 65 (1979). This work deals with commensurate-incommensurate transitions; domain walls in their problem correspond to steps on crystal surfaces in our work. The SOS conditions forbid step crossings; this no-crossing condition is the essence of the Pokrovsky-Talapov transition.

[8]This exponent corresponds to an exponent $\alpha=\frac{1}{2}$ for a transition associated with the (100) face of a simple-cubic crystal studied by H. W. J. Blöte and H. J. Hilhorst, J. Phys. A **15**, L631 (1982). The exponent $\frac{3}{2}$ first appears implicitly in a calculation for fcc crystals by E. E. Gruber and W. W. Mullins, J. Phys. Chem. Solids **28**, 875 (1967). These authors found the $\frac{3}{2}$ analytically only at low temperatures and did not recognize its connection with a critical exponent.

[9]C. Rottman, M. Wortis, J. C. Heyraud, and J. J. Metois, Phys. Rev. Lett. **52**, 1009 (1984).

[10]F. Gallet, P. E. Wolf, and S. Balibar (unpublished).

[11]See, e.g., L. D. Landau and E. M Lifshitz, *Statistical Physics* (Addison-Wesley, Reading, Mass., 1969), Sec. 143.

[12]J. W. Cahn and D. W. Hoffman, Acta Metall. **22**, 1205 (1974).

[13]N. Cabrera, Surf. Sci. **2**, 320 (1964).

[14]A. F. Andreev, Zh. Eksp. Teor. Fiz. **80**, 2042 (1981) [Sov. Phys.—JETP **53**, 1063 (1982)].

[15]See, e.g., E. H. Lieb and F. Y. Wu, in *Phase Transitions and Critical Phenomena,* edited by C. Domb and M. S. Green (Academic, London, 1972), Vol. 1.

[16]B. Sutherland, C. N. Yang, and C. P. Yang, Phys. Rev. Lett. **19**, 588 (1967). See also C. P. Yang, *ibid.* **19**, 586 (1967); C. Jayaprakash and A. Sinha, Nucl. Phys. B **210** [FS6], 93 (1982).

[17]R. J. Baxter, *Exactly Solved Models in Statistical Mechanics* (Academic, New York, 1982).

[18]J. K. MacKenzie, A. J. W. Moore, and J. F. Nicholas, J. Chem. Phys. Solids **23**, 185 (1962). We have corrected a misprint in their result [their Eq. (21)].

[19]C. Herring, Phys. Rev. **82**, 87 (1951).

[20]H. van Beijeren, Phys. Rev. Lett. **38**, 993 (1977).

[21]Technically, the SOS condition can be imposed by introducing anisotropic nearest-neighbor bonds, and letting those bonds with components normal to the surface in question go to infinity. This device is a bit unphysical, and we shall merely assume that voids and overhangs are not crucial to the qualitative physics at all T and, in particular, are irrelevant, in the renormalization-group sense, near second-order phase transitions in the ECS.

[22]An equivalent expression is terms of the principal "macroscopic surface stiffnesses" Γ_x and Γ_y is $(\Gamma_x\Gamma_y)^{1/2}=\pi k_B T/2d^2$. Γ_x and Γ_y appear, for $T>T_R$, in the free energy $f(\vec{s})$ as $f(\vec{s})=f_0+\frac{1}{2}(\Gamma_x s_x^2+\Gamma_y s_y^2)$. See D. S. Fisher and J. D. Weeks, Phys. Rev. Lett. **50**, 1077 (1983).

[23]See, e.g., F. Wegner, in *Phase Transitions and Critical Phenomena,* edited by C. Domb and M. S. Green (Academic, London, 1972), Vol. 1.

[24]See, e.g., D. J. Bishop and J. D. Reppy, Phys. Rev. Lett. **40**, 1727 (1978); D. R. Nelson and J. M. Kosterlitz, *ibid.* **39**, 1201 (1977).

[25]H. J. F. Knops, Phys. Rev. Lett. **39**, 766 (1977).

[26]Equation (22) of the text for the curvature is just a simple transcription to our notation of the result [Eq. (345a) of Ref. 15], $\chi=A(T-T_c)^{-1}+\cdots$, for the electric polarizability of the ferroelectric six-vertex model as the ferroelectric transition is approached from above.

[27]H. J. Schulz, Phys. Rev. B **22**, 5274 (1980).

[28]C. Herring, in *Structure and Properties of Solid Surfaces,* edited by R. Gomer and C. S. Smith (University of Chicago Press, Chicago, 1953), Chap. 1.

[29]J. S. Rowlinson and B. Widom, *Molecular Theory of Capillarity* (Clarendon, Oxford, 1982).

[30]G. Agnolet, S. Teitel, and J. D. Reppy, Phys. Rev. Lett. **47**, 1537 (1981).

[31]Note that the quadratic term in Eq. (27), valid for $T<T_R$, and the quadratic term in Eq. (38), valid for $T>T_R$, are not clearly related as $T\to T_R$. This is because the domain of validity of the series of Eq. (27) becomes vanishingly small as $T\to T_R$. The related problem of the crossover from the Pokrovsky-Talapov behavior to the roughening behavior near but above T_R is quite interesting and remains unsolved.

[32]C. N. Yang and C. P. Yang, Phys. Rev. **150**, 327 (1966). See their Eq. (69) and our Ref. 16. See also B. Horovitz, T. Bohr, J. M. Kosterlitz, and H. J. Schulz, Phys. Rev. B **28**, 6596 (1983).

[33]This is a simple transcription of the corresponding result for superfluid films quoted in Ref. 30.

[34]J. C. Heyraud and J. J. Metois, Acta Metall. **28**, 1789 (1980); J. Cryst. Growth **50**, 571 (1980).

[35]C. Jayaprakash, C. Rottman, and W. F. Saam (unpublished).

[36]V. I. Marchenko and A. Ya Parshin, Zh. Eksp. Teor. Fiz. **79**, 257 (1980) [Sov. Phys.—JETP **52**, 129 (1980)]. Here we refer to steps of the same sign.

[37]V. I. Marchenko, Zh. Eksp. Teor. Fiz. **81**, 1141 (1981) [Sov. Phys.—JETP **54**, 605 (1981)].